Journal of Solid State Chemistry 182 (2009) 3358–3364

Contents lists available at ScienceDirect

Journal of Solid State Chemistry

journal homepage: www.elsevier.com/locate/jssc

Evidence of local defects in the oxygen excess apatite $La_{9.67}(SiO_4)_6O_{2.5}$ from high resolution neutron powder diffraction

Stéphanie Guillot [a], Sophie Beaudet-Savignat [a,*], Sébastien Lambert [a], Rose-Noelle Vannier [b], Pascal Roussel [b], Florence Porcher [c]

[a] CEA Le Ripault, BP 16, 37260 Monts, France
[b] Unité de Catalyse et de Chimie du Solide, Equipe de Chimie du Solide, UMR CNRS 8181, ENSCL-Université des Sciences et Technologies de Lille, 59652 Villeneuve d'Ascq, France
[c] Laboratoire Léon Brillouin, CEA Saclay, 91191 Gif sur Yvette, France

ARTICLE INFO

Article history:
Received 26 June 2009
Received in revised form
25 September 2009
Accepted 26 September 2009
Available online 2 October 2009

Keywords:
Apatite
Electrolyte
SOFC
Neutron diffraction
Conduction mechanism

ABSTRACT

From neutron diffraction data collected at 3 K on a powder of $La_{9.67}(SiO_4)_6O_{2.5}$ composition and a careful examination of the average structure, a model was proposed to explain the oxygen over-stoichiometry in the apatite structure. This model leads to realistic distances to neighbouring atoms. Moreover, it accounts perfectly for the maximum oxygen content observed in these materials. Up to 0.5 oxygen atom located at the vicinity of the 2*a* site (0, 0, $\frac{1}{4}$) would be shifted to a new interstitial position in the channel at (−0.01, 0.04, 0.06), creating a Frenkel defect, with the possibility of a maximum occupancy in this site equal to twice the Frenkel defect numbers. This structural model is in good agreement with the oxygen diffusion pathways recently proposed by Bechade et al. (2009) using computer modeling techniques. It supports preferred oxygen diffusion pathways via interstitial oxygen atoms and vacant sites along [0 0 1], close to the centre of the La(2)-O channels.

1. Introduction

Research on oxide ion conductors for solid oxide fuel cell (SOFC) applications has dramatically increased over the past few decades. Today, the commercial electrolyte used in SOFCs is yttria stabilised zirconia (YSZ) [2,3]. However, in order to achieve sufficient oxide ion conductivity, this electrolyte requires high temperatures (900–1000 °C) which imply the use of expensive interconnect materials and leads to a premature aging of the cell components.

Therefore, in the last years, one of the principal research axes was focused on the development of new electrolyte materials which could be employed at lower temperatures, around 700 °C. Several types of oxide ion conductors were investigated: among these, perovskite-type oxides such as doped $LaGaO_3$ [4,5], gadolinium doped ceria [6,7], or rare earth oxyapatites. The latter were reported by Nakayama et al. [8,9]. Since then, they have generated considerable interest for their high level of ionic conductivity at "moderate temperature" and also for their good chemical stability. Their general formula is $Ln_{10-x}\square_x(SiO_4)_6O_{2\pm\delta}$ where *Ln* is a rare earth element. Their structure consists of isolated $[SiO_4]^{4-}$ tetrahedra with *Ln* cations located in two sites, a 7-coordinated one and a 9-coordinated one, and two extra oxide ions occupying channels along the *c*-axis (Fig. 1). It is well described in the $P6_3/m$ space group, with La(1) in 4*f* ($\frac{1}{3}$, $\frac{2}{3}$, $z\sim0$), La(2) in 6*h* ($x\sim0.01$, $y\sim0.24$, $\frac{1}{4}$), Si in 6*h* ($x\sim0.40$, $y\sim0.37$, $\frac{1}{4}$), O(1) in 6*h* ($x\sim0.32$, $y\sim0.48$, $\frac{1}{4}$), O(2) in 6*h* ($x\sim0.59$, 0.47, $\frac{1}{4}$), O(3) in 12*i* ($x\sim0.34$, $y\sim0.25$, $z\sim0.07$), O(4) in 2*a* (0, 0, $\frac{1}{4}$) [10]. Other space groups, *P*-3 [11] and $P6_3$ [12–15], were proposed leading to very close structural models.

The initial studies were performed on $Ln_{10}(SiO_4)_6O_2$ where *Ln*=La, Nd, Sm, Gd, Dy [8,9,16]. As the best conducting properties were obtained for *Ln*=La, subsequent studies mainly focused on lanthanum oxyapatites. It was demonstrated that the apatite structure could accept a wide range of partial substitutions on the Si and La sites. Solid solutions with Al [17–24], Ga [25], Mg [15,24–26] and Ge [27,28] on the Si site and with Ca, Sr, Ba, Mg [29–32] were reported. Mg is a special case since, as an ambisite, it can substitute either for Si or La [15]. Possibility of cation vacancy was also clearly evidenced, these vacancies being mainly located on the La(1) site [12,33,34].

Depending on the cation stoichiometry, oxygen deficient ($\delta<0$), stoichiometric ($\delta=0$) or oxygen excess apatites ($\delta>0$) are obtained. It is now clear that their ionic conductivity depends directly on the oxygen content and consequently on the cation stoichiometry. For instance, $La_8Sr_2(SiO_4)_6O_2$ exhibits a lower conductivity and a higher activation energy than compositions containing lanthanum vacancies, such as $La_{9.33}(SiO_4)_6O_2$, or

* Corresponding author.
E-mail address: sophie.beaudet-savignat@cea.fr (S. Beaudet-Savignat).

0022-4596/$ - see front matter © 2009 Elsevier Inc. All rights reserved.
doi:10.1016/j.jssc.2009.09.031

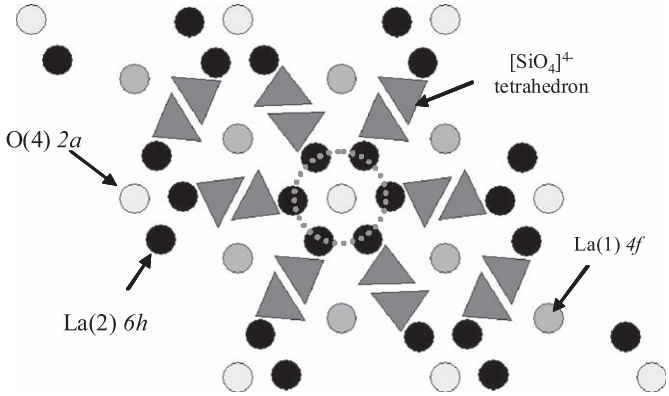

Fig. 1. Structure of $La_{10-x}\square_x(SiO_4)_6O_{2\pm\delta}$.

oxygen excess such as $La_9Sr_1(SiO_4)_6O_{2.5}$ [11,29]. Our previous studies showed that compositions which display, at the same time, oxygen excess ($\delta > 0$) and are doped with an alkaline-earth element such as Sr^{2+} or Ba^{2+} on the La site, exhibit better conduction properties. Conductivity higher than $10^{-2}\,S\,cm^{-1}$ at 700 °C was measured for $La_9Ba_1(SiO_4)_6O_{2.5}$ [30,35].

If these materials were confirmed to be pure oxide ion conductors, their conduction mechanism is still a subject for controversy. An interstitial oxygen mechanism is admitted but the location of this oxygen and the migration pathways remain badly known.

In 2003, for the first time, using atomistic simulation technique, Tolchard et al. proposed the existence of an interstitial oxygen site lying at the channel periphery at (0.01; 0.23; 0.60) (very close to one of the oxygen site belonging to the SiO_4 tetrahedra ~1 Å) for $La_{9.33}Si_6O_{26}$ [36,37]. They predicted an interstitial migration via a nonlinear (sinusoidal-like) pathway along the *c*-axis, facilitated by local cooperative relaxation of the SiO_4. More recently, a similar study on the oxygen excess composition $La_{9.67}Si_6O_{26.5}$ led to the same conclusions [38]. In addition, it was proposed that the presence of interstitial oxide ions would create "SiO_5" units. This hypothesis was supported by ^{29}Si NMR, which shows the existence of more than one silicate environment [39]. This interstitial site was confirmed by neutron powder diffraction in various apatite compositions and for different temperatures [14,15,23,33,40,41] although it remains very close to the O(3) site (0.73 Å for $La_{9.33}Si_6O_{26}$ [33]) which precludes their simultaneous occupancy. In all these studies, the possibility of a local relaxation, i.e. displacement of tetrahedra was argued. However, this site was not systematically evidenced, authors did not detect any extra oxygen [10,42,43] or a random distribution around the La(2) site was proposed [44]. A position closer to the centre of the channel was found for compositions $La_{8.65}Sr_{1.35}(SiO_4)_6O_{2.32}$ and $La_9Sr_1(SiO_4)_{5.5}(AlO_4)_{0.5}O_{2.25}$ [22]. Such a position was recently confirmed by Bechade et al. for composition $La_{9.33}(SiO_4)_6O_2$ [1]. Using atomic scale computer modeling techniques, they proposed the existence of an interstitial site in the conduction channels located in (0.106, 0.0177, 0.588). The oxygen diffusion would occur by a push-pull type mechanism including cooperative displacements of interstitial oxide ions and channel oxide ions O(2*a*) with more realistic distances to neighbouring atoms.

With the aim to investigate the local structure and to locate the interstitial oxygen atoms in the structure, in this paper, powder neutron diffraction was carried out on the oxygen excess apatite $La_{9.67}(SiO_4)_6O_{2,5}$. Data were collected at 3, 100 and 300 K. From these low temperature data, a minimisation of the dynamic disorder, i.e. the thermal displacement, was expected which should facilitate the localisation of the extra oxygen atoms in the structure.

2. Experimental section

2.1. Synthesis

The $La_{9.67}(SiO_4)_6O_{2.5}$ apatite was prepared by high temperature solid state reaction from stoichiometric amounts of La_2O_3 (Rhodia 99.99%) and amorphous SiO_2 (Cerac 99.99%). The La_2O_3 and SiO_2 powders were first annealed at 1100 °C in order to achieve complete decarbonation and dehydroxylation. Stoichiometric amount of the starting materials was then ball milled during 24 h in ethanol, before being dried and dry ground. In order to obtain the pure apatite powders required for neutron powder diffraction, the mixture was directly calcinated at 1625 °C in air. Heating and cooling rates were 150 °C/h.

The obtained powder chemical composition was confirmed by inductively coupled plasma spectrometry. The experimental values, 69.1 ± 2.8 and 8.6 ± 0.9 wt% for La and Si, respectively, were in good agreement with the expected values: 69.4 and 8.7 wt %, respectively. In addition, electron probe microanalysis and transmission electron microscopy energy dispersive spectrometry analysis were performed on dense ceramics. They showed good composition homogeneity and no secondary phase at the grain boundary.

To check the possibility of protons in the sample, Solid State NMR was carried out on an Avance 400 WB Bruker spectrometer (9.4 T) but no signal was evidenced.

2.2. Characterisations

Phase purity was controlled by X-ray diffraction at room temperature (Siemens D5000–Cu*K*α1 diffractometer). XRD patterns were analysed with EVA [45] and JANA2000 [46] softwares.

Neutron powder diffraction (NPD) experiments were carried out at the Orphée reactor of the Léon Brillouin Laboratory (CEA/Saclay-France), on the high resolution 3T2 diffractometer using Ge(335) monochromator and a wavelength $\lambda = 1.2251$ Å. Data were measured at 3, 100 and 300 K, in the $10^\circ < 2\theta < 120^\circ$ range with a 0.05° step. The JANA2000 software [46] was used for the Rietveld refinement of data.

3. Results

With the aim to precisely locate the interstitial oxygen atoms expected by the chemical composition of the studied apatite, the low temperature data were refined in a first step. A structural model was deduced, and introduced in the refinement of the data collected at 100 and 300 K, in a second step. Comparisons of the calculated and experimental NPD patterns are given in Fig. 2. They show a good agreement between the calculated and experimental data.

3.1. Refinements of 3 K NPD data

To start the refinement of the 3 K data, the structural model of apatite without interstitial oxygen atom [10] was introduced. The three space groups: $P6_3/m$ ($n°176$), $P6_3$ ($n°173$) and $P\text{-}3$ ($n°147$) were tested. Since there was no significant difference between the *R*-factors, less correlations and less parameters for $P6_3/m$ (69 atomic parameters for $P\text{-}3$ and $P6_3$ against 44 for $P6_3/m$), this space group was chosen for the following refinements. It was further supported by the fact Matsushita et al. did not evidence

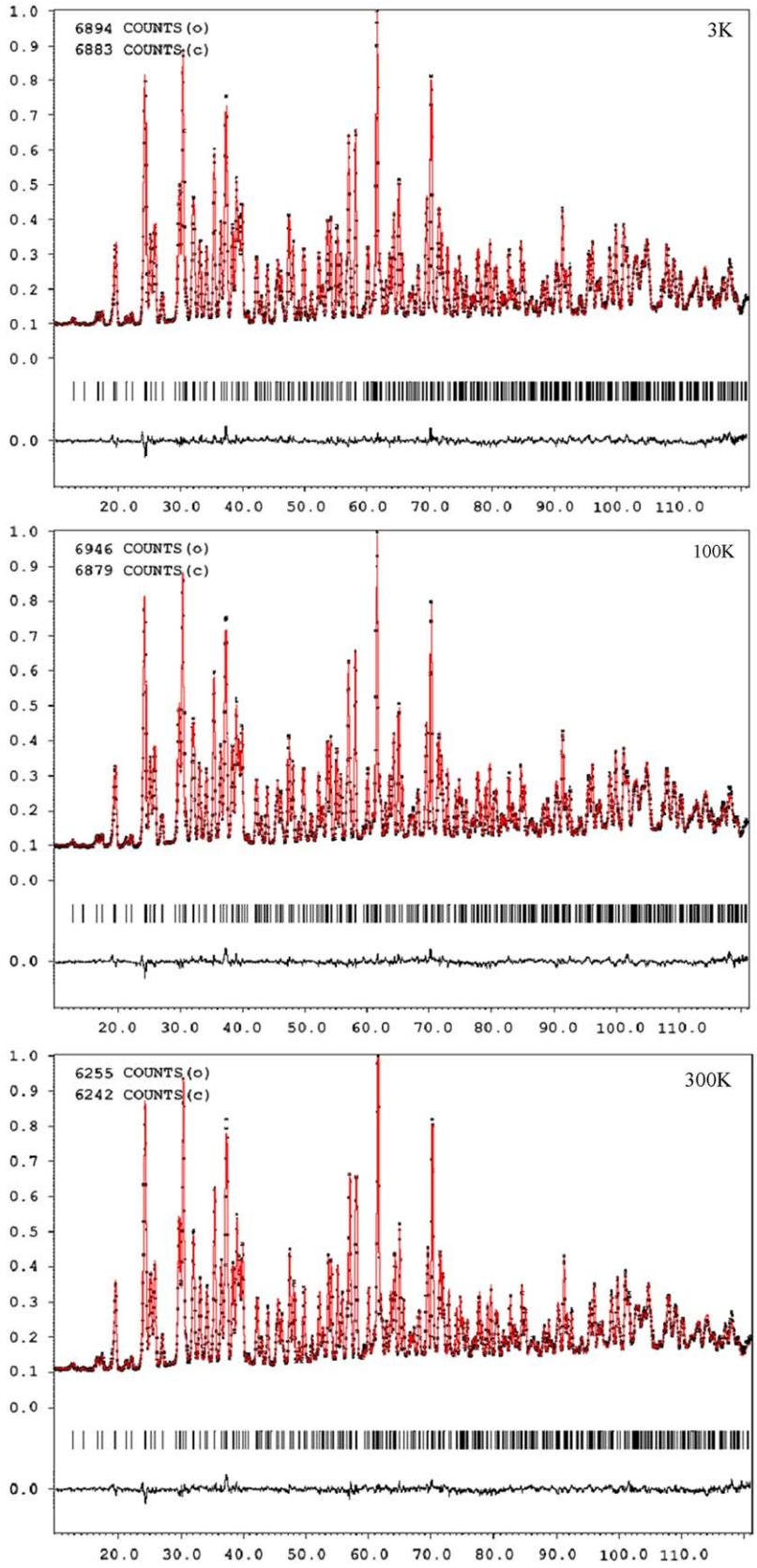

Fig. 2. Calculated neutron powder diffraction patterns compared to experimental data collected at 3, 100 and 300 K on $La_{9.67}(SiO_4)_6O_{2.5}$.

any secondary harmonic generation signal for a close composition [44]. Reliability factors of R_{obs}=2.11%, R_{wobs}=2.11%, R_p=2.34%, R_{wp}=2.95% and R_{exp}=1.27% were obtained at this stage (see Table 1). They show a good matching between the experimental pattern and the calculated one. The refined structural data and the associated interatomic distances are reported in Tables 2 and 3.

Table 1
Refined parameters from NPD data collected on "$La_{9.67}(SiO_4)_6O_{2.5}$".

	3 K	100 K	300 K
a (Å)	9.705(1)	9.707(1)	9.719(2)
C (Å)	7.1787(8)	7.1798(8)	7.185(2)
Without O(5)			
R_{obs}/R_{wobs}	2.11/2.11	2.26/2.15	2.30/2.24
R_p/R_{wp}	2.34/2.95	2.36/2.94	2.29/2.88
With O(5)			
R_{obs}/R_{wobs}	2.03/1.91	2.22/2.03	2.23/2.00
R_p/R_{wp}	2.26/2.80	2.30/2.84	2.13/2.61

As observed at room temperature in the previous studies, a high anisotropic spread of the nuclear density along [001] direction was observed for the O(4) site, located at the centre of the channels of the structure, leading to a high U_{33} ADPs value, U_{33}=0.22(2) Å^2. Refinement of occupancy led to 5% of oxygen vacancy on this site. At such a very low temperature, dynamic disorder is very low and such a high ADPs value can only be explained by a static disorder from the ideal position (0,0,$\frac{1}{4}$). In contrast, the Si site displayed a localised nuclear density with low ADPs. Inside the tetrahedra, the mean Si–O distance was close to 1.62 Å which is in good agreement with what is expected from the sum of Si and O radii. This result confirms the tetrahedra rigidity which is also characterised by anisotropic oxygen thermal displacements, more pronounced for the O(3) site which exhibits higher ADPs in the [1 0 0] direction. The La(2) site is fully occupied and, as shown in previous studies [12,34,35], lanthanum vacancies were evidenced in the La(1) site with a site occupancy of 0.88(1). Taking into account this occupancy, the sample composition should be $La_{9.52}(SiO_4)_6O_{2.28}$ instead of $La_{9.67}(SiO_4)_6O_{2.5}$. Despite the lower La content, oxygen excess (δ=0.28) was therefore expected. However, in a first analysis, it was not possible to locate any extra oxide ion on the Fourier difference map. At this stage, the commonly admitted position located at (−0.01; 0.23; 0.60) [36] was introduced in the refinement but it led to no convergence.

Then, to check the possibility to introduce new oxygen atoms in the structure, a research of cavities was performed from these NPD data, using the ATOMS software [47]. This approach takes into account the average position of the atoms in the structure, not the thermal displacements. A drawing of the cavities is given in Fig. 3. The biggest cavity was found in the conduction channel at (0.06, 0.10, 0), at 2.0(1) and 2.3(2) Å from O(4) and O(3), respectively (Fig. 3). The size of this cavity is slightly smaller than the size of an oxide ion. However, the presence of interstitial oxygen in this site is possible with a local relaxation of the structure.

To try to evidence residual nucleon density in this area, the Fourier difference was then examined again at another scale. A spread positive residual density was found at (−0.01, 0.04, 0.06). To improve the contrast and thus observe this residue on the Fourier map, the nuclear density from z=0.02 to 0.10 was summed up (Fig. 4). This position is far from the oxygen sites belonging to the SiO_4 tetrahedra, the closest site being O(3) at a distance of at least 2.74 Å. However, at a distance of 1.47 Å, it is too close to O(4) and precludes a simultaneous occupancy of O(4) and the new interstitial site. However, the distance between two symmetrical interstitial sites by the mirror symmetry, being of 2.75 Å, a simultaneous occupancy of two interstitial sites could be possible. Therefore, one O(4) site located on the mirror at z=0.25, could be replaced by two interstitial sites at z=0.06 and 0.44. These two sites would be at only 2.28 Å from the next O(4) which is a little short but, as written above, O(4) exhibits a static disorder and is likely not located on the mirror. A slight shift of O(4) out of the mirror to $z\sim$0.28 would increase the distance from 2.28 to 2.48 Å

Table 2
"$La_{9.67}(SiO_4)_6O_{2.5}$" refined structural data, ADPs parameters in Å^2.

	3 K Without O(5)		3 K With O(5)	100 K	300 K
La(1), 4*f*, ($\frac{1}{3}$, $\frac{2}{3}$, z)					
Occup	0.88(1)		0.88(1)	0.88(1)	0.88(1)
z	−0.0011(8)		−0.0011(7)	−0.0004(8)	−0.0001(2)
U_{11}	0.004(1)		0.004(1)	0.005(1)	0.009(1)
U_{33}	0.018(3)		0.017(2)	0.010(2)	0.022(2)
U_{eq}	0.011(1)		0.009(1)	0.010(1)	0.013(1)
La(2), 6*h*, (x, y, $\frac{1}{4}$)					
X	0.2277(4)		0.2279(3)	0.2276(4)	0.2276(3)
Y	−0.0122(4)		−0.0121(4)	−0.0123(4)	−0.0119(4)
U_{11}	0.006(2)		0.005(1)	0.007(2)	0.011(1)
U_{22}	0.002(1)		0.002(1)	0.003(1)	0.006(1)
U_{33}	0.005(1)		0.006(1)	0.006(2)	0.010(1)
U_{12}	0.000(1)		0.001(1)	0.002(1)	0.004(1)
U_{eq}	0.005(1)		0.004(1)	0.006(1)	0.009(1)
Si, 6*h*, (x, y, $\frac{1}{4}$)					
x	0.4021(8)		0.4027(7)	0.4025(7)	0.4023(6)
y	0.3722(7)		0.3728(6)	0.3725(7)	0.3724(6)
U_{11}	0.003(3)		0.003(2)	0.006(3)	0.008(2)
U_{22}	0.010(3)		0.011(3)	0.010(3)	0.011(3)
U_{33}	0.005(3)		0.002(2)	0.004(3)	0.006(2)
U_{12}	0.002(3)		0.003(2)	0.004(3)	0.005(2)
U_{eq}	0.006(2)		0.005(2)	0.006(2)	0.009(2)
O(1), 6*h*, (x, y, $\frac{1}{4}$)					
x	0.3236(6)		0.3232(5)	0.3233(6)	0.3237(5)
y	0.4851(7)		0.4848(6)	0.4852(7)	0.4856(6)
U_{11}	0.018(3)		0.019(2)	0.022(3)	0.030(2)
U_{22}	0.016(3)		0.017(3)	0.010(3)	0.026(3)
U_{33}	0.013(3)		0.015(3)	0.016(4)	0.020(2)
U_{12}	0.015(2)		0.017(2)	0.020(2)	0.025(2)
U_{eq}	0.013(2)		0.013(2)	0.015(2)	0.020(2)
O(2), 6*h*, (x, y, $\frac{1}{4}$)					
X	0.5962(5)		0.5965(5)	0.5967(5)	0.5964(4)
y	0.4744(6)		0.4740(5)	0.4740(6)	0.4734(5)
U_{11}	0.007(3)		0.008(2)	0.009(2)	0.012(2)
U_{22}	0.006(2)		0.006(2)	0.006(2)	0.009(2)
U_{33}	0.014(3)		0.014(3)	0.016(3)	0.021(3)
U_{12}	0.001(2)		0.003(2)	0.003(2)	0.003(2)
U_{eq}	0.009(2)		0.010(2)	0.011(2)	0.015(2)
O(3), 12*i*, (x, y, z)					
x	0.3473(5)		0.3472(3)	0.3472(5)	0.3464(4)
y	0.2557(4)		0.2558(4)	0.2558(4)	0.2560(3)
z	0.0684(4)		0.0681(4)	0.0683(4)	0.0687(4)
U_{11}	0.040(3)		0.040(2)	0.042(3)	0.049(2)
U_{22}	0.011(2)		0.011(2)	0.012(2)	0.015(2)
U_{33}	0.008(2)		0.008(1)	0.008(2)	0.011(1)
U_{12}	0.015(2)		0.014(2)	0.014(2)	0.016(2)
U_{13}	−0.013(2)		−0.012(2)	−0.013(2)	−0.015(1)
U_{23}	−0.004(1)		−0.004(1)	−0.004(1)	−0.005(1)
U_{eq}	0.019(2)		0.020(2)	0.020(2)	0.025(2)
O(4), 2*a*, (0,0, $\frac{1}{4}$)		O(4), 4*e*, (0,0,z)			
Occup	0.95(1)	Occup	0.40(1)	0.40(1)	0.40(1)
U_{11}	0.004(4)	z	0.282(2)	0.282(2)	0.282(2)
U_{33}	0.22(2)	U_{iso}	0.01	0.01	0.02
U_{eq}	0.081(7)				
O(5), 12i, (x, y, z)					
		Occup	0.057(3)	0.059(4)	0.057(4)
		x	0.01(2)	−0.01(2)	−0.03(1)
		y	0.027(9)	−0.02(1)	0.106(5)
		z	0.112(4)	0.113(5)	0.02
		U_{iso}	0.01	0.01	0.02

Symmetry gives the following restrictions: $U_{11}=U_{22}=2U_{12}$ for the sites La(1) and O(4) (in 2*a* site), $U_{13}=U_{23}=0$ for the others sites except O(3). The refinement led to the following formula: $La_{9.52}(SiO_4)_6O_{2.28}$.

Table 3
"$La_{9.67}(SiO_4)_6O_{2.5}$" selected interatomic distances (Å).

		3 K Without O(5)	3 K With O(5)	100 K	300 K
La(1)	O(1) [× 3]	2.489(6)	2.490(6)	2.484(6)	2.485(5)
	O(2) [× 3]	2.544(6)	2.540(5)	2.542(6)	2.546(5)
	O(3) [× 3]	2.841(6)	2.842(5)	2.844(5)	2.856(4)
La(2)	O(1)	2.758(8)	2.754(7)	2.756(7)	2.767(6)
	O(2)	2.507(6)	2.510(5)	2.512(6)	2.521(5)
	O(3) [× 2]	2.605(5)	2.606(4)	2.608(5)	2.608(4)
	O(3) [× 2]	2.470(4)	2.468(4)	2.469(4)	2.473(3)
	O(4)	2.272(4)	2.284(4) [× 2]	2.283(4) [× 2]	2.284(4) [× 2]
	O(5)		2.3(2)	2.31(15)	2.38(16)
	O(5)		2.58(18)	2.45(16)	2.38(13)
	O(5)		2.62(12)	2.7(2)	2.7(2)
Si	O(1)	1.617(11)	1.617(10)	1.622(11)	1.622(9)
	O(2)	1.632(8)	1.630(7)	1.634(7)	1.632(6)
	O(3) [× 2]	1.631(5)	1.635(4)	1.632(5)	1.631(4)
O(4)	La(2) [× 3]	2.272(5)	2.284(4)	2.283(4)	2.284(4)
	O(4)		0.460(17)	0.462(10)	0.467(16)
	O(5) [× 3]		*0.80*(5)	*0.79*(7)	*0.82*(7)
	O(5) [× 3]		*1.24*(6)	1.24(5)	1.27(4)
	O(5) [× 3]		2.38(4)	2.39(4)	2.36(4)
	O(5) [× 3]		2.84(4)	2.85(4)	2.80(4)
O(5)	O(3)		2.91(19)	2.84(12)	2.78(11)
	O(3)		2.95(14)	–	–
	O(5) [× 2]		*0.4*(3)	*0.4*(2)	0.5(2)
	O(5) [× 2]		*1.62*(6)	1.64(6)	1.54(2)
	O(5)		*1.67*(7)	1.70(8)	1.61(9)
	O(5)		*1.98*(5)	1.96(6)	2.07(5)
	O(5) [× 2][a]		2.03(8)	2.01(8)	2.12(9)

Distances in italic corresponds to two sites that cannot be simultaneously occupied.

[a] The refinement led to underestimated O(5)–O(5) distances. From Fourier map a more realistic distance of 2.75Å is expected.

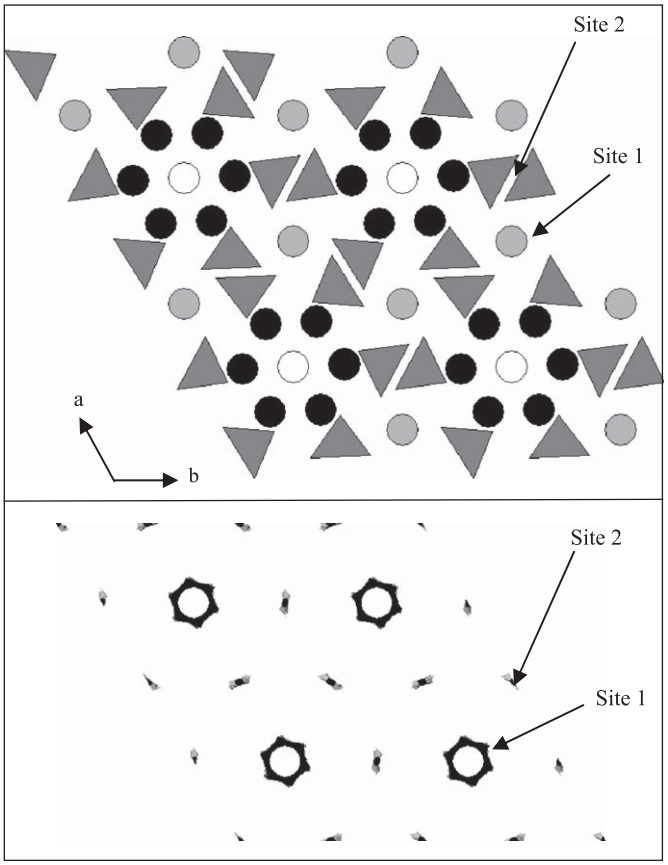

Fig. 3. Cavities plot in the "$La_{9.67}(SiO_4)_6O_{2.5}$" structure after refinement without interstitial oxygen. The biggest cavity is evidenced at (0.06, 0.10, 0), site 1. The site 2, (0, 0.48, 0.50) is too small to accept an oxygen atom.

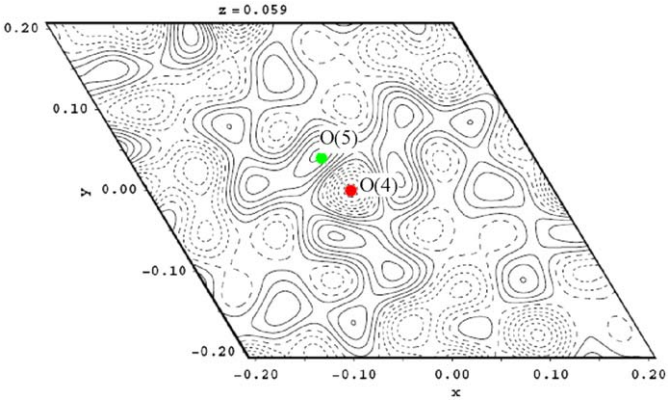

Fig. 4. Fourier difference map without O(5) at 3 K showing the interstitial oxygen. For a better contrast, the nucleon density was sum from *z* between 0.02 and 0.10 (solid lines represents positive density and dashed lines represents negative density). The contour is 0.5 n/Å^3.

and allow the simultaneous occupancy of these O(4) sites and the interstitial sites. Fig. 5 show the structural defect position. This model allows the possibility to accommodate the over-stoichiometry without any problem of neighbouring distances and demonstrates the possibility of interstitial oxygen atoms in the structure.

These positions were then introduced in the refinement. O(4) was split in a 4*e* site and the oxygen excess was introduced in a 12*i* O(5) site at (−0.01, 0.04, 0.06). The sum of O(4) and O(5) sites occupancy was constrained to the oxygen stoichiometry derived from the cation occupancy. Since the simultaneous refinement of occupancy and thermal parameters of these two sites was not possible, because of too high correlations, the thermal displacement of these two sites was fixed at U_{iso}=0.01Å^2. This value is in the same order of magnitude than the displacement observed for the other oxygen sites. If in a second time, we refined U_{iso} for O(4) and O(5) fixing the occupation, the refinement led to values close to the value we had fixed. Results of this new refinement are given in Tables 1 and 2. A significant decrease of the *R* factors was observed (R_{obs}=2.03%, R_{wobs}=1.91%, R_p=2.26%, R_{wp}=2.80%) supporting this model.

O(4) and O(5) converged to (0, 0, 0.282(2)) and (0.01(2), 0.027(9), 0.112(4)), respectively. According to our hypothesis, O(5) cannot be occupied more than twice the number of O(4) vacancy. Interestingly, the refinement led to 0.68 oxygen in O(5) (5,7% occupancy) against 1.60 atoms in O(4), in good agreement with our hypothesis. However, the *z* coordinate of O(5) shifted to 0.11 which leads to a too short O(5)–O(5) distance to allow the simultaneous occupation of two interstitial sites. But, with such a low occupancy, the accuracy of the refinement for the O(5) position is rather low and the true position is more likely at (−0.01; 0.04; 0.06), the position which was evidenced in the Fourier difference map.

3.2. Refinements of 100 and 300 K NPD data

The same model was then introduced in the refinement of data collected at 100 and 300 K. Because of the increase of thermal

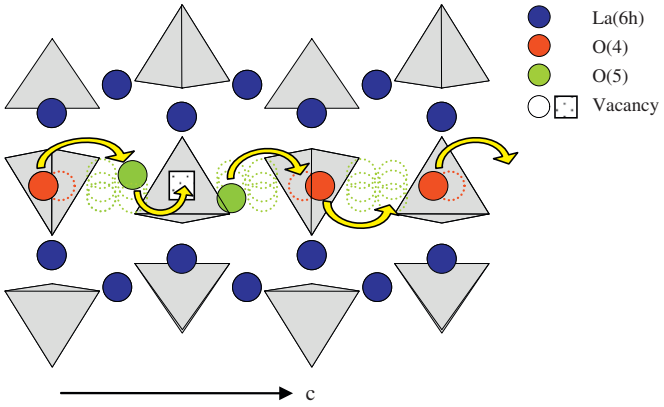

Fig. 5. Structural defect position and possible conduction mechanism along the *c* axis (representation of two adjacent unit-cells).

parameters with temperature, at 300 K, the thermal displacements of O(4) and O(5) sites were fixed at U_{iso}=0.02 Å^2. The refinement, in the two cases, led to an O(5) site at the same position (Table 2). Here also, the reliability factors, presented in Table 1, are slightly better for the model including the O(5) site. No significant structural modification was evidenced with the temperature (considering the atomic positions, ADPs and interatomic distances) (Table 3).

4. Discussion

Interstitial oxygen was evidenced by Fourier map at (−0.01; 0.04; 0.06). This position is close to the position proposed by Bechade et al. (0.0177, −0.0883, 0;088) [1]. It is also in good agreement with the position found by Leon Reina et al. for $La_9Sr_1(SiO_4)_{5,5}(AlO_4)_{0,5}O_{2.25}$ at 300 K [22] and $La_{8.65}Sr_{1.35}(SiO_4)_6O_{2.32}$ at 4 K [33], with interstitials at (0.015(18), 0.064(8), 0.537(9)) (i.e. −0.015(18), −0.064(8), 0.037(9)) and (0.018(10), 0.050(6), 0.573(7)) (i.e. −0.018(10), −0.050(6), 0.073(7)), respectively. From a distance point of view, the occupation of this site is possible only if the O(4) site is vacant. One O(4) can be replaced by two interstitial oxygen atoms, creating a complex defect ($\ddot{V}_O, 2O''$), as proposed by Bechade et al. [1].

The refinement led to the effective composition $La_{9.52}(SiO_4)_6O_{2.28}$ with 0.68 oxygen in O(5) against 1.60 atoms in O(4), confirming the existence of vacancies on the O(4) site. At the most, one oxygen could be introduced in O(5) for 0.5 vacancy in O(4).

Our structural model supports Bechade et al. modelling and the conduction mechanism they proposed [1]. Oxide ion diffusion would occur in the channel along [001] via the O(5) and O(4) sites by an interstitial/vacancy mechanism. More precisely, an interstitial oxygen O(5) is supposed to move first from an O(5) interstitial site to an adjacent O(4) vacancy. This motion implies the displacement of the other interstitial oxygen O(5), located on the other side of the O(4) vacancy, to a new interstitial position and the displacement of the nearest O(4) atom to an adjacent interstitial position (Fig. 5). In this way, distances between O(4) and O(5) always remain higher than 2.5 Å, which is the minimal distance commonly admitted in oxide structures.

5. Conclusion

The structure of a pure apatite powder $La_{9.67}(SiO_4)_6O_{2.5}$ was investigated by neutron powder diffraction at 3, 100 K and room temperature. In a first step, a structural model without interstitial oxygen atom was introduced in the refinement. Refinement of atom occupancy led to the following composition: $La_{9.52}(SiO_4)_6O_{2.28}$ which implied extra oxygen in the structure. Research of cavities in the structure revealed space at (0.06, 0.10, 0), which was confirmed by Fourier difference calculation which revealed residual density at (−0.01, 0.04, 0.06). Taking into account this interstitial site, a structural model with realistic distances was proposed. The O(4) site, located at the vicinity of the (0, 0, $\frac{1}{4}$) site is shift to a 4e site at z=0.28, it is locally replaced by, at the most, two O(5) sites in these interstitial positions. The conduction mechanism would occur via these interstitial O(5) atoms and O(4) vacancies along [001] in agreement with the recent results published by Bechade et al. [1].

Acknowledgments

The authors are grateful to Julien Trebosc for ^{1}H NMR. The Laboratoire Léon Brillouin is gratefully acknowledged for neutron facilities.

References

[1] E. Bechade, O. Masson, T. Iwata, I. Julien, K. Fukuda, E. Champion, Chem. Mater. 21 (2009) 2508–2517.
[2] B.C.H. Steele, Solid State Ionics 134 (2000) 3–20.
[3] V.V. Kharton, F.M.B. Marques, A. Atkinson, Solid State Ionics 174 (2004) 135–149.
[4] A. Ahmad-Khanlou, F. Tietz, D. Stöver, Solid State Ionics 135 (2000) 543–547.
[5] K.C. Wincewicz, J.S. Cooper, J. Power Sources 140 (2005) 280–296.
[6] S.C. Singhal, Solid State Ionics 152 (2002) 405–410.
[7] B.C.H. Steele, A. Heinzel, Nature 414 (2001) 345–352.
[8] S. Nakayama, T. Kageyama, H. Aono, Y. Sadaoka, J. Mater. Chem. 5 (1995) 1801–1805.
[9] S. Nakayama, H. Aono, Y. Sadaoka, Chem. Lett. 6 (1995) 431–432.
[10] Y. Masubuchi, M. Higuchi, T. Takeda, S. Kikkawa, Solid State Ionics 177 (2006) 263–268.
[11] J.E.H. Sansom, D. Richings, P.R. Slater, Solid State Ionics 139 (2001) 205–210.
[12] S. Lambert, A. Vincent, E. Bruneton, S. Beaudet-Savignat, F. Guillet, B. Minot, F. Bouree, J. Solid State Chem. 179 (2006) 2602–2608.
[13] J.R. Tolchard, J.E.H. Sansom, M.S. Islam, P.R. Slater, Dalton Trans. (2005) 1273–1280.
[14] E. Kendrick, M.S. Islam, P.R. Slater, Solid State Ionics 177 (2007) 3411–3416.
[15] E. Kendrick, J.E.H. Sansom, J.R. Tolchard, M.S. Islam, P.R. Slater, Faraday Discuss. 134 (2007) 181–194.
[16] S. Nakayama, M. Sakamoto, J. Eur. Ceram. Soc. 18 (1998) 1413–1418.
[17] E.J. Abram, D.C. Sinclair, A.R. West, J. Mater. Chem. 11 (2001) 1978–1979.
[18] V. Kahlenberg, H. Krüger, Solid State Sci. 6 (2004) 553–560.
[19] A.L. Shaula, V.V. Kharton, F.M.B. Marques, J. Solid State Chem. 178 (2005) 2050–2061.
[20] S. Chefi, A. Madani, H. Bousseta, C. Roux, A. Hammou, J. Power Sources 177 (2008) 464–469.
[21] A. Mineshige, T. Nakao, M. Kobune, T. Yazaw, H. Yoshioka, Solid State Ionics 179 (2008) 1009–1012.
[22] N. Takeda, Y. Itagaki, H. Aono, Y. Sadaoka, Sensors Actuators B 115 (2006) 455.
[23] L. Leon-Reina, J.M. Porras-Vazquez, E.R. Losilla, M.A.G. Aranda, Solid State Ionics 177 (2006) 1307–1315.
[24] H. Yoshioka, J. Am. Ceram. Soc. 90 (10) (2009) 3099–3105.
[25] J.E.H. Sansom, J.R. Tolchard, P.R. Slater, M.S. Islam, Solid State Ionics 167 (2004) 17–22.
[26] H. Yoshioka, S. Tanase, Solid State Ionics 176 (2005) 2395–2398.
[27] J.E.H. Sansom, P.R. Slater, Solid State Ionics 167 (2004) 23–27.
[28] J.E.H. Sansom, A. Najib, P.R. Slater, Solid State Ionics 175 (2004) 353–355.
[29] P.R. Slater, J.E.H. Sansom, Solid State Phenom. 90 (2003) 195–200.
[30] S. Beaudet-Savignat, A. Vincent, S. Lambert, F. Gervais, J. Mater. Chem. 17 (2007) 2078–2087.
[31] A. Najib, J.E.H. Sansom, J.R. Tolchard, P.R. Slater, M.S. Islam, Dalton Trans. (2004) 3106–3109.
[32] L.W. Schroeder, M. Mathew, J. Solid State Chem. 26 (1978) 383–387.
[33] L. Leon-Reina, J.M. Porras-Vazquez, E.R. Losilla, D.V. Sheptyakov, A. Llobet, M.A.G. Aranda, Dalton Trans. (2007) 2058–2064.
[34] J. Felsche, J. Solid State Chem. 5 (1972) 266–275.
[35] A. Vincent, S. Beaudet-Savignat, F. Gervais, J. Eur. Ceram. Soc. 27 (2007) 1187–1192.
[36] J.R. Tolchard, M.S. Islam, P.R. Slater, J. Mater. Chem. 13 (2003) 1956–1961.
[37] M.S. Islam, J.R. Tolchard, P.R. Slater, Chem. Commun. (2003) 1486–1487.

[38] A. Jones, P.R. Slater, M.S. Islam, Chem. Mater. 20 (2008) 5055–5060.
[39] J.E.H. Sansom, J.R. Tolchard, M.S. Islam, D. Apperley, P.R. Slater, J. Mater. Chem. 16 (2006) 1410–1413.
[40] L. Leon-Reina, E.R. Losilla, M. Martinez-Lara, S. Bruque, M.A.G. Aranda, J. Mater. Chem. 14 (2004) 1142–1149.
[41] L. Leon-Reina, E.R. Losilla, M. Martinez-Lara, S. Bruque, A. Llobet, D.V. Sheptyakov, M.A.G. Aranda, J. Mater. Chem. 15 (2005) 2489–2498.
[42] H. Okudera, Y. Masubuchi, S. Kikkawa, A. Yoshiasa, Solid State Ionics 176 (2005) 1473–1478.
[43] T. Iwata, K. Fukuda, E. Béchade, O. Masson, I. Julien, E. Champion, P. Thomas, Solid State Ionics 178 (2007) 1523–1529.
[44] Y. Matsushita, F. Izumi, K. Kobayashi, N. Igawa, H. Kitazawa, Y. Oyama, S. Miyoshi, S. Yamaguchi, Nucl. Instrum. Methods Phys. Res. A 600 (2009) 319–321.
[45] 〈http://www.bruker.axs.de/eva.html〉.
[46] V. Petricek, M. Dusek, L. Palatinus, Jana2000 The crystallographic computing system, Institute of Physics, Praha, Czech Republic, 2000.
[47] 〈http://www.shapesoftware.com〉.